First Test Results Of MIMOSA-26, A Fast CMOS Sensor With Integrated Zero Suppression And Digitized Output

J. Baudot, G. Bertolone, A. Brogna, G. Claus, C. Colledani, Y. Değerli, R. De Masi, A. Dorokhov, G. Dozière, W. Dulinski, M. Gelin, M. Goffe, A. Himmi, F. Guilloux, C. Hu-Guo, K. Jaaskelainen, M. Koziel, F. Morel, F. Orsini, M. Specht, I. Valin, G. Voutsinas, M. Winter

***Abstract*—The MIMOSA pixel sensors developed in Strasbourg have demonstrated attractive features for the detection of charged particles in high energy physics. So far, full-size sensors have been prototyped only with analog readout, which limits the output rate to about 1000 frames/second.**

The new MIMOSA 26 sensor provides a 2.2 cm^2 sensitive surface with an improved readout speed of 10,000 frames/second and data throughput compression. It incorporates pixel output discrimination for binary readout and zero suppression micro-circuits at the sensor periphery to stream only fired pixel out. The sensor is back from foundry since february 2009 and has being characterized in laboratory and in test beam. The temporal noise is measured around 13-14 e$^-$ and an operation point corresponding to an efficiency of 99.5$\pm$0.1 % for a fake rate of 10^{-4} per pixel can be reached at room temperature.

MIMOSA 26 equips the final version of the EUDET beam telescope and prefigures the architecture of monolithic active pixel sensors (MAPS) for coming vertex detectors (STAR, CBM and ILC experiments) which have higher requirements. Developments in the architecture and technology of the sensors are ongoing and should allow to match the desired readout speed and radiation tolerance.

Finally, the integration of MAPS into a micro-vertex detector is addressed. A prototype ladder equipped, on both sides, with a row of 6 MIMOSA 26-like sensors is under study, aiming for a total material budget about 0.3% X$_0$.

I. Introduction

CMOS sensors provide a unique combination of features as low mass pixel detectors with respect to other technologies. They offer a high granularity and a thin sensitive volume, combined with the possibility to integrate read-out micro-circuits on the same substrate as the sensing element. Without increasing the material budget, the latter allows specific read-out strategies targeted for a given application. The MIMOSA 26 sensor is the first large scale sensor from the MIMOSA [1] series [1], to profit fully from this advantage. Indeed, the chip incorporates signal discrimination and zero-suppression logic to deliver a binary output. It has been designed to equip the high resolution beam telescope developed within the EUDET consortium [2].

This telescope, made of two arms of 3 reference planes, requires highly granular and thin pixel detectors to provide a track extrapolation in the middle of the telescope with an uncertainty around 2 μm. The reference detectors have to cover a sensitive area of more than 2 cm^2 to be read 10 thousand times per second and to cope with a rate of 10^6 particles/cm^2/s.

Such specifications are similar to those of some micro-vertex detectors for which MIMOSA 26 is or could be a forerunner. The STAR experiment at the Brookhaven National Laboratory is upgrading its inner detector (Heavy Flavor Tracker [3]) with CMOS sensors having a 200 μs read-out time for a sensitive surface close to 4 cm^2 and a pixel pitch of 18.4 μm. The radiation tolerance required is in the range of a few kGy and a fluence of 3.10^{12} n$_{eq}$/cm^2. Additionally, the maximum power dissipation allowed is 100 mW/cm^2 and the targeted material budget of one single layer of pixel sensor is 0.3% X$_0$.

Longer term projects include vertex detectors for the CBM experiment [4] at the FAIR facility of the GSI and the ILD [5] experiment at the future ILC. There are notable deviation in the specifications with respect to the EUDET or HFT projects. The read-out time should decrease down to 25 μs or below for the innermost layer of an ILC vertex detector and even down to around 10 μs for the CBM front layer with respect to the beam. Also, the particle rate reached at this CBM front pixel layer requires a tolerance up to 10^{14} n$_{eq}$/cm^2 and several 10 kGy.

MIMOSA 26 was designed in 2008 and back from foundry early in 2009. It has already been delivered to EUDET for a first data taking campaign during the second half of 2009. The next session of this paper describes the architecture of the sensor, while the following ones discuss its extensive tests in laboratory and in beam. The two last sections focus on the sensor developments necessitated by the coming projects (STAR, CBM and ILD) and adress the issue of the integration of such sensors in ultra-low mass detector.

II. MIMOSA 26 architecture

The MIMOSA 26 chip realize a comprehensive charge sensing and signal read-out chain, providing discriminated

Manuscript received November 4, 2007.

J. Baudot, G. Bertolone, A. Brogna, G. Claus, C. Colledani, R. De Masi, A. Dorokhov, G. Dozière, W. Dulinski, M. Goffe, A. Himmi, C. Hu-Guo, K. Jaaskelainen, M. Koziel, F. Morel, M. Specht, I. Valin, G. Voutsinas and M. Winter are with IPHC, Université Louis Pasteur, CNRS/IN2P3, BP 28, F-67037 Strasbourg, France (telephone: +33 388 106 632, e-mail: baudot@in2p3.fr).

Y. Değerli, M. Gelin, F. Guilloux and F. Orsini are with IRFU-SEDI, CEA-Saclay, F-91191 Gif-sur-Yvette, France (e-mail: fabienne.orsini@cea.fr).

[1]standing for Minimum Ionizing MOS Active pixel sensor.

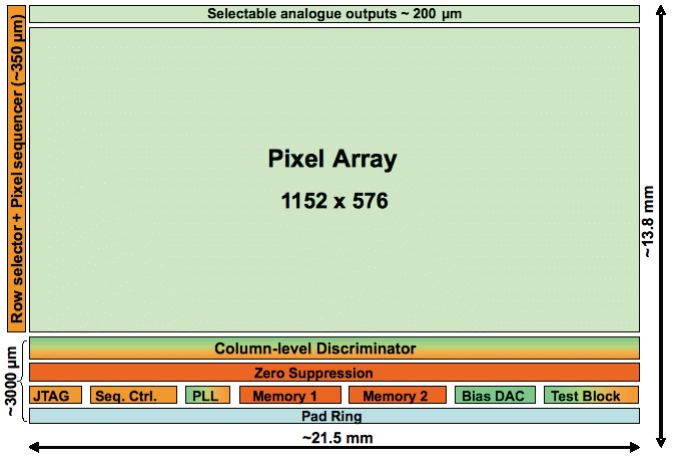

Fig. 1. Schematic view of the MIMOSA 26 displaying the different functional blocks.

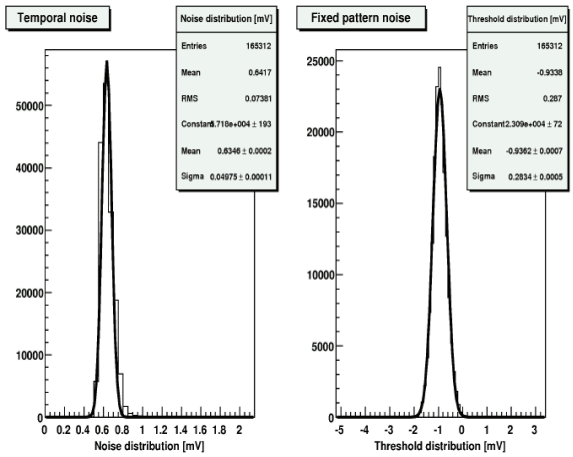

Fig. 2. Noise distribution over a quarter of the sensitive surface as measured at a 80 MHz clock frequency.

signals in a binary mode including the pixel address. It was fabricated in the AMS 0.35 μm OPTO technology.
The pixel matrix is composed of about 0.7 million of pixels: 1152 columns and 576 rows (18.4 μm pitch). Rows are read one by one in a rolling shutter mode while amplification and correlated double sampling is implemented inside each pixel. This strategy allows to digitize the pixel signal, after a second column double sampling, with an offset compensated discriminator terminating each column. At a 80 MHz clock frequency, the whole pixel matrix is read out in 112 μs.
The binary outputs of the discriminator are piped-line into a zero suppression logic which scans the sparse row data and stores in embedded memories the address and length of consecutive fired pixels. Up to 9 such groups can be loaded per row. The memories are serially read out with two 80 Mbits/s outputs. The data compression factor typically ranges between 10 to 10000, depending on the occupancy level.

The sensor layout is pictured in figure 1 where the dimensions of the insensitive areas appear. The 200 μm wide top band serves only test purposes (analog readout of pixels) and can be removed for any vertex detector application. The thin 350 μm side band dedicated to the row steering which will eventually be moved at the chip bottom. It remains all the micro-circuits for the discrimination, zero-suppression, slow-control (biasing through DAC and JTAG controller) and pad ring, which occupy a 3000 μm width.

The MIMOSA 26 sensor actually combines the architecture of two earlier prototypes: MIMOSA 22 [6] and SUZE 01 [7] fabricated in 2007 /2008 and tested in 2008. The small scale (128 columns of 576 pixel rows) MIMOSA 22 sensor validated the in pixel correlated double sampling and column-end discrimination. The zero-suppression logic and memories read-out was tested with the SUZE 01 chip, designed for the output of 128 columns.
Special emphasis was put on the chip testability. Specific outputs were designed to access individually the analog pixel output, the discriminator stage, the zero-suppression logic and the serial outputs. Test results are discussed in the next section.

III. Test results

Around 30 MIMOSA 26 sensors have been tested in different conditions (temperature was usually stabilized around 20°C). The yield for functional sensors having less than 0.5 % of dead pixels, reaches 90 %.

In laboratory, all the test facilities were used to validate the chip operation.
An ^{55}Fe source allowed to calibrate the equivalent noise charge (ENC) of the analog pixel output to be below 14 e^- at a 80 MHz clock frequency. The charge collection was also measured, with the X-rays (5.9 and 6.5 keV), to be identical to the one of MIMOSA 22, reaching an efficiency of 22 % for the seed pixel and 86 % for an array of 5×5 pixels.
Noise estimation was performed for individual discriminator (by group of 288) not connected to pixels by varying a unique threshold for all discriminators. The same technics was repeated to evaluate the overall noise (pixel + discriminator) of individual channels. The ENC amounts to 12 and 13 e^-, at a 80 MHz clock frequency, equivalent to those found for the smaller matrix of MIMOSA 22. The fixed pattern noise contribution, 0.3-0.4 mV, is dominated by the discriminator dispersion; while the temporal noise, ranging between 0.6 and 0.7 mV, comes mainly from the pixel behavior. The distribution of these noises over a quarter of the sensor is illustrated on figure 2.
The suppression logic was tested with millions of input patterns up to a frequency of 115 MHz. Finally, the static power dissipation amounts to 300 mW which has to be understood as 520μW per column (i.e. increasing the number of lines does not increase this power). A 1 % occupancy level induces a dynamic power dissipation of 200 mW.

Six MIMOSA 26 sensors have been mounted in a telescope-like structure and bombarded with 120 GeV π^- at the CERN-SPS. Tracks were reconstructed using five of the sensors while the measurements from the middle one

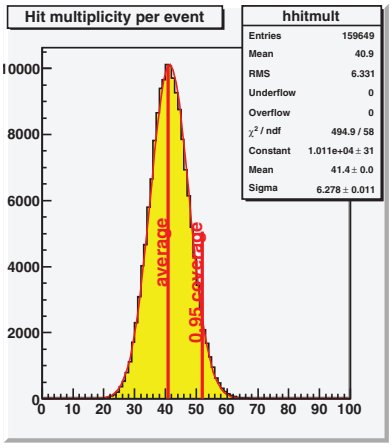

Fig. 3. Distribution of the number of fake hits per event for the full matrix of MIMOSA 26, over around 160 000 events.

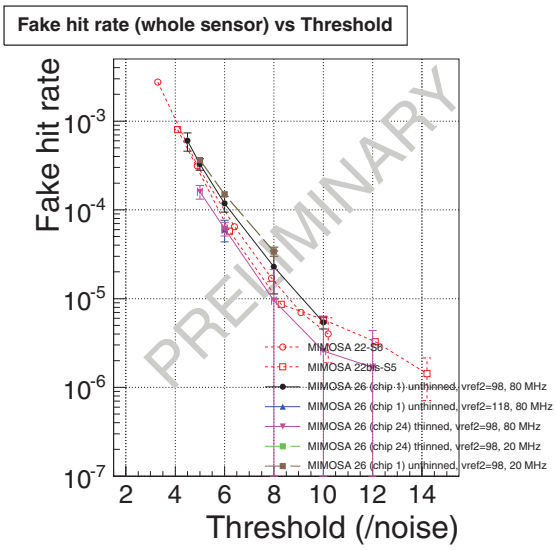

Fig. 4. Evolution of the fake hit rate averaged over the full matrix with respect to the threshold, unique for all the discriminators.

were compared to the track extrapolation. A few millions of triggers were acquired with varying the incidence angle from 90 to 30 degrees. Results discussed below are the preliminary analysis outputs of the normal incidence data.

We studied in detail the fake hit rate in the absence of beam and found that the number of fake hits per event on the whole matrix follows a gaussian distribution, see figure 3. There is an important dispersion of the level of fake rate among pixels, nevertheless the few pixels with a high rate do not perturbate (saturation) the sensor operation in the zero-suppression mode down to a discriminator threshold equivalent to 5 times the noise. At a threshold of 6 times the noise, the fraction of pixels firing more than once every 100 events was found to be less than 0.2%. The evolution of the fake hit rate per pixel with the threshold is represented on figure 4 for different sensors and different frequencies, along with the MIMOSA 22 reference.

The reference tracks allow to estimate the detection

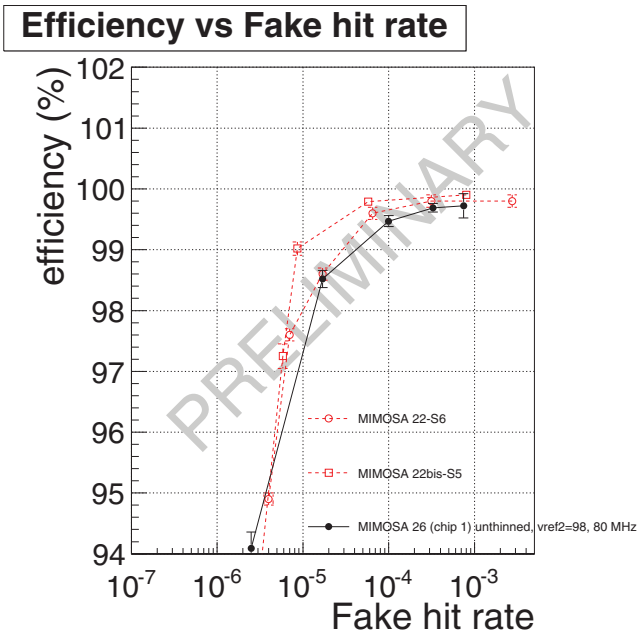

Fig. 5. Different efficiency-average fake hit rate operation points reached as obtained for Mimosa 26 compared to small-size circuits (Mimosa 22 and 22bis).

efficiency by counting the number of tracks matching a hit in the tested device. Hits are associated with a track if they fall in a circle of 50 μm radius around the track extrapolation. Obviously, the efficiency depends on the discriminator threshold and hence is related to the fake hit rate per pixel, see figure 5. The measured efficiency is satisfactory compared to the one observed with MIMOSA 22 and amounts to 99.5$\pm$0.1% for an average fake hit rate of 10^{-4} per pixel.

The spatial resolution estimation is also made possible with the reference tracks, using the residual distribution between the track extrapolation and the associated hit position. The current result is still preliminary and appears to deviate by +0.5 μm with respect to the 3.5 μm measured resolution of MIMOSA 22, almost irrespective of the threshold set on the discriminators. Two reasons may be invoked to explain this observation. First, the algorithm to estimate the hit position, from the geometry of the cluster of pixels fired by the same particle, is still not optimized. Second, inhomogeneities in the cluster shape due to the dispersion of the noise over the large number of pixels may degrade the resolution. With five sensors used as reference planes, the uncertainty on the track extrapolation in the middle of the telescope was estimated at 2.1$\pm$0.4 μm.

As a conclusion, the three main figures, fake hit rate, efficiency and spatial resolution match the expectation for the exploitation of MIMOSA 26 in the EUDET telescope.

IV. Ongoing developments

As stated in the introduction, the requirements for the STAR pixel detector are similar to those of EUDET. The final sensor for this application, ULTIMATE, will be fabricated in

2010 and will mainly consists in an extension of the sensitive surface of MIMOSA 26. But future experiments (CBM, ILD) call for faster sensor and/or a higher radiation-tolerance. Several ongoing developments target these improvements.
First the readout architecture of MIMOSA 26 will be transform such as to reproduce the discrimination and zero-suppression micro-circuits on both sides of the sensor. Each side reads then half of the pixel matrix and the readout speed is doubled by this parallelization.
It is also foreseen to replace the discrimination stage with a digitization, each column being equipped with one few-bits (4 to 5) analog to digital converter. The additional precision on the pixel level allow to increase the pixel pitch while keeping the same (or better) spatial resolution. Indeed the impact position estimation improves when using the charge center of gravity for instance. So, with less pixels to read per unit area, a better compromise between readout speed and sensitive surface can be reached.

Deeply sub-micron CMOS processes, with a feature size $\leq$0.18 μm, offer several improvements at once, keeping the same architecture as MIMOSA 26. Due to smaller micro-circuits for the same function, the insensitive area can be reduced. The operating frequency, hence readout speed, is increased thanks to smaller capacitance of metal lines. And finally, the power dissipation usually decreases with lower voltage used in these processes.
Another current evolution of the technology will be beneficial mostly for radiation tolerance. High-resistivity substrates, i.e. low-doped epitaxial layer, starts to be available at certain founders. As already demonstrated [8], some level of depletion is reached within such sensitive volumes, which makes the charge collection faster and more focussed on a few pixels. These two phenomena alleviate the decrease of the signal which occurs after non-ionizing radiation. An improvement by, at least, an order of magnitude on neutron equivalent fluence tolerance is expected.
All these development lines are expected to lead the MIMOSA sensors to approach the desired performances in 3 to 4 years.

Finally, a longer term development concerns the use of the so-called 3D integration technologies which allow the pixel to pixel connection of two chips or sensors from different wafers. As a consequence, future sensors will incorporate several layers, each of them being dedicated to a given function and using the optimal technology for it. This concept offers potentially the best performances possible. First steps in this direction have started in 2009 [9], [10]

V. Integration studies

The final performances of a given detector results from the combination of the characteristics of both the sensitive element and the integration system (mechanics, electrical servicing, ...). For a vertex detector, the main point of the integration is to allow sufficient mechanical stability to benefit from the sensor intrinsic spatial resolution while keeping the material budget low. The physics goals at the ILC require that a single layer of the vertex detector provides two measurement points with a single point resolution better than 3 μm for each and that the material budget of this double sided layer stays below 0.3% X_0.
We have initiated a project called PLUME which is addressing these unprecedented specifications for sensor integration, and targets to build a demonstrator ladder by 2012. The ladder design is based on a thin silicon carbide (SiC) foam supporting six sensors thinned to around 50 μm on each of its sides, to form a 1×12 cm^2 sensitive area. The sensor are themselves connected to a low mass flex cable providing electrical power, control and readout. Air cooling of the system is expected to be sufficient to cope with the power dissipation of the sensors.
In 2009, first prototypes have been built using analog readout sensors MIMOSA 20 which have a 1×2 cm^2 sensitive area. Two 50 μm thick chips have been bonded on a flex cable. This flex cable was designed by the University of Frankfurt as a prototype for the CBM experiment and was not optimized for material budget. A ladder is made of a 2 mm thick SiC with one equipped flex mounted on each side. Its material budget amounts to about 0.6% X_0 equivalent thickness. Tests in the SPS beam at CERN are being conducted in November 2009 to evaluate the benefit of the double position information provided by such a ladder with respect to the pointing accuracy.
The next prototype will include six MIMOSA 26 sensors and reach the scale required by a vertex detector and is already being designed to be fabricated early in 2010. This double sided ladder will be operated in the power-pulsing mode, suited to the ILC beam time-structure, in order to save power and will be air-cooled. Test campaigns are foreseen to monitor the thermal distribution, mechanical stability and signal over noise ratio during operation. Several prototypes will follow to ultimately match the ILC material budget requirements. They will also be used in beam test to demonstrate the feasibility of the alignment of such ladders.

VI. conclusion

The MIMOSA 26 sensor has been designed as the final detector of the EUDET beam telescope project. With more than 2 cm^2 sensitive area, its performances match the ones of its smaller prototype predecessors, offering 99.5$\pm$0.1 % efficiency for MIP at a fake hit rate of 10^{-4} per pixel and sustaining 10^6 particles/cm^2/s. These performances allow its straighforward extension for the PIXEL vertex detector for the STAR experiment in 2010.

On top of this, the architecture offers a natural baseline for more demanding applications in therms of readout speed and radiation tolerance. Finally, the program to demonstrate the possibility to integrate such sensors in a real vertex detector keeping the benefit of the thin sensitive volume and single point resolution of monolithic pixel sensors has started.

References

[1] M. Winter, *Development of Swift, High Resolution, Pixel Sensor Systems for a High Precision Vertex Detector suited to the ILC Running Conditions*, DESY PRC R&D Nr 01/04, November 2009.

[2] I. Gregor on behalf of the EUDET Consortium, *The EUDET Infrastructures for Detector R&D*, contribution N45-2 in these proceedings.
[3] M.Szelezniak *et al.*, *CMOS pixel vertex detector at STAR*, Proceedings of Science (VERTEX-08, 28 July-1 August, 2008,Utö Island, Sweden) 032.
[4] M.Deveaux *et al.*, *Challenges with decay vertex detection in CBM using an ultra-thin pixel detector system linked with the silicon tracker*, Proceedings of Science (VERTEX-08, 28 July-1 August, 2008,Utö Island, Sweden) 028.
[5] A.Besson *et al.*, *CMOS sensors for the vertex detector of the future international linear collider*, Nucl. Inst. Meth. **A 572** (2007) 300.
[6] Ch.Hu-Guo *et al.*, *CMOS pixel sensor development: a fast read-out architecture with integrated zero suppression*, Journal of Instrumentation-JINST 4 (2009) P04012.
[7] A.Himmi *et al.*, *A Zero Suppression Micro-Circuit for Binary Readout CMOS Monolithic Sensors*, Proceedings of the TWEPP 2009 workshop, Paris, 21-25 September 2009.
[8] A.Dorokhov *et al.*, *Improved radiation tolerance of MAPS using a depleted epitaxial layer*; Presented at the 11th European Symposium on Semiconductor Detectors , Wildbad Kreuth, 7-11 June 2009.
[9] W.Dulinski *et al.*, *Thin, Fully Depleted Monolithic Active Pixel Sensor with Binary Readout based on 3D Integration of Heterogeneous CMOS Layers*, contribution N22-5 in these proceedings.
[10] Y.Değerli *et al.*, *A Vertically Integrated (3D) Rolling Shutter Mode MAPS with in-Pixel Digital Memory and Delayed Readout*, contribution N25-167 in these proceedings.